



Oblique Wave Trapping by a Surface-Piercing Flexible Porous Barrier in the Presence of Step-Type Bottoms

H. Behera^{1,2} · S. Ghosh^{1,2,3}

Received: 21 September 2017 / Accepted: 8 January 2018 / Published online: 13 September 2018
© Harbin Engineering University and Springer-Verlag GmbH Germany, part of Springer Nature 2018

Abstract

The present study deals with the oblique wave trapping by a surface-piercing flexible porous barrier near a rigid wall in the presence of step-type bottoms under the assumptions of small amplitude water waves and the structural response theory in finite water depth. The modified mild-slope equation along with suitable jump conditions and the least squares approximation method are used to handle the mathematical boundary value problem. Four types of edge conditions, i.e., clamped-moored, clamped-free, moored-free, and moored-moored, are considered to keep the barrier at a desired position of interest. The role of the flexible porous barrier is studied by analyzing the reflection coefficient, surface elevation, and wave forces on the barrier and the rigid wall. The effects of step-type bottoms, incidence angle, barrier length, structural rigidity, porosity, and mooring angle are discussed. The study reveals that in the presence of a step bottom, full reflection can be found periodically with an increase in (i) wave number and (ii) distance between the barrier and the rigid wall. Moreover, nearly zero reflection can be found with a suitable combination of wave and structural parameters, which is desirable for creating a calm region near a rigid wall in the presence of a step bottom.

Keywords Oblique incident wave · Wave trapping · Surface-piercing · Flexible porous barrier · Mild-slope approximation · Least squares approximation

1 Introduction

Over the past few decades, the problem of wave interaction with vertical porous barriers is of considerable interest to the scientific community for the protection of offshore facilities from different wave attacks. Various analytical, numerical, and experimental approaches have been performed to investigate the importance of vertical porous barriers with different configurations. The study on wave interaction with a

perforated wall breakwater started after Jarlan (1961). Since then, various modified Jarlan-type breakwaters have been proposed and investigated for reducing wave force depending on applications. Sahoo et al. (2000) studied the wave trapping by a partial porous barrier near a rigid wall using the least squares approximation method. They found that the curves of reflection coefficients are periodic and each curve repeats itself in every half-wavelength, which is similar to that of a fully submerged porous barrier studied by Chwang and Dong (1984). Li et al. (2003) conducted a research on the reflection of oblique incident waves by breakwaters with double-layered perforated walls. They observed that if a single-layered perforated caisson could reduce the wave reflection notably, it is not necessary to place a second perforated wall in such a single-perforated caisson. Nevertheless, if the single-layered perforated caisson produces little reduction on wave reflection, installing a second perforated wall can significantly reduce the wave reflection. Liu et al. (2007a) examined the wave interaction with a new modified perforated breakwater, consisting of a perforated front wall, a solid back wall, and a wave-absorbing chamber between them with a two-layer rock-filled core. The reflection of oblique waves

✉ H. Behera
hkb.math@gmail.com

S. Ghosh
sukhendu.math@gmail.com

¹ SRM Research Institute, SRM Institute of Science and Technology, Kattankulathur, Tamil Nadu, India

² Department of Mathematics, SRM Institute of Science and Technology, Kattankulathur, Tamil Nadu, India

³ NLPCU, Faculty of Sciences, Université libre de Bruxelles, Brussels, Belgium

from a structure consisting of an infinite array of partially perforated caissons was also investigated by Liu et al. (2007b). A thorough review of the developments on wave interaction with various perforated breakwaters can be found in Huang et al. (2011) and the literature cited therein.

On the other side, there is a wide interest on wave interaction with flexible porous structures as these structures are light in weight, economical, reusable, and environmentally friendly. These kinds of structures are often used for temporary protection of coastal infrastructures/facilities and in construction sites. For example, the use of flexible barriers for chord grass seedling, oil spilling, and pollution control is well studied in the literature. Williams (1996) investigated the hydrodynamic properties of a flexible floating breakwater consisting of a membrane structure attached to a small float restrained by moorings. Cho et al. (1998) developed an analytical solution to study oblique wave interaction with a dual vertical flexible membrane wave barrier hinged at the seafloor in the context of the two-dimensional linear wave-body interaction theory. Moreover, they have compared the analytical results with their developed boundary element method results. Using eigenfunction expansions for the velocity potential and linear membrane theory, Lo (1998) studied the performance of a wave barrier consisting of two vertical flexible membranes spaced at a fixed distance apart. Later, Lo (2000) investigated the interaction of water waves with a vertical flexible membrane of a finite extent which is less than the water depth. Yip et al. (2002) studied wave trapping by a partial flexible porous barrier near a rigid wall. Behera et al. (2013) investigated the performance of a partial flexible porous structure on wave trapping in a two-layer fluid. Karmakar et al. (2013) investigated gravity wave scattering by multiple surface-piercing floating porous membranes. Later, Karmakar and Soares (2014) considered oblique wave scattering by multiple bottom-standing flexible porous barriers by using the least squares method. Recently, using Green's function technique, Koley et al. (2015) investigated the effects of a bottom-standing and surface-piercing flexible porous plate on wave scattering. Afterwards, Kaligatla et al. (2015) have extended their study on wave trapping by a vertical submerged flexible porous plate located near a vertical rigid wall. Most recently, Koley and Sahoo (2017) investigated oblique wave trapping by vertical permeable membrane barriers located near a wall.

In the aforementioned studies, the problems are considered in the case of uniform water depth or in the presence of a vertical step. However, there are few studies on wave interaction with vertical partial structures near a rigid wall in the presence of a step-type bottom bed. Using the Galerkin eigenfunction method, an analytical model has been developed by Suh and Park (1995) to predict the reflection coefficient of a perforated wall caisson mounted on a rubble mound foundation when waves are obliquely incident to the

breakwater at an arbitrary angle. Using the extended modified mild-slope equation along with suitable jump conditions developed by Porter and Staziker (1995), Behera et al. (2015) investigated wave trapping by a fully extended porous barrier near a rigid wall in the presence of an undulated bottom. Later, Behera et al. (2016) studied wave scattering by a bottom-standing flexible porous barrier in the presence of various step bottoms. However, there is a negligible number of investigations on wave trapping by single/double flexible permeable/impermeable barriers near a rigid wall in the presence of an undulated bottom.

In the current study, wave interaction with a surface-piercing flexible porous barrier near a rigid wall is considered in the presence of sloping step-type bottoms. To determine the velocity potential in an undulated region, the modified mild-slope equation as in Porter and Staziker (1995) is used and solved by using the Runge-Kutta method, while the eigenfunction expansion method is used to find out the velocity potentials in the fluid domain having a uniform water depth. It is worth pointing out that although the modified mild-slope approximation method is a classic one, it still has to be used properly in various mathematical models in order to achieve the solution efficiently. Moreover, the least squares approximation method is used for finding the solutions in the presence of a partial surface-piercing flexible porous barrier. To keep the barrier at a desired position of interest, clamped-moored, clamped-free, moored-free, and moored-moored edge conditions are considered. The effects of the step bottom, porous-effect parameter and rigidity of the flexible barriers, oblique angle of incidence, and other wave and structural parameters are analyzed on wave reflection, free surface elevations, and wave forces on the barrier as well as the rigid wall.

2 Mathematical Formulation

Oblique wave trapping by a surface-piercing flexible porous barrier near a rigid wall in the presence of an undulated bottom bed is investigated under the assumptions of the linearized water wave theory and small amplitude structural response. The problem is considered in the three-dimensional Cartesian coordinate system with $x-y$ being the horizontal plane and the z -axis being the vertically downward negative direction as in Fig. 1. It is apprehended that the undulated bottom bed occupies the region $0 < x < L$ with variable depth $h(x)$ and the uniform open water regions $-\infty < x < 0$ and $L < x < \infty$ with constant water depths h_1 and h_2 , respectively. The flexible porous barrier of length a is located at a distance D and L_1 from the rigid wall and end edge of the step, respectively. The fluid is supposed to be extended horizontally along the y -axis over $y < \infty$. Assuming that the fluid is inviscid and incompressible, and the motion is irrotational

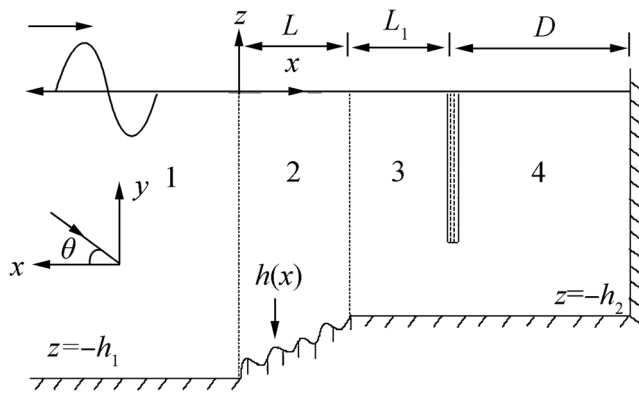


Fig. 1 Schematic diagrams of wave interaction with a flexible porous barrier near a rigid wall

and simple harmonic in time with angular frequency ω , the form of the velocity potential for four different regions with $j = 1, 2, 3, 4$ is given by $\Phi_j(x, y, z, t) = \text{Re} \left\{ \phi_j(x, z) e^{-i(k_y y + \omega t)} \right\}$, where θ is the incidence angle with the x -axis and $k_y = k_{10} \sin \theta$ with k_{10} being the wave number of the incident wave in region 1. $H_b = (-a, 0)$ and $H_g = (-h_2, -a)$ denote the regions of the barrier and the gap along the vertical z -direction, respectively. The spatial velocity potential $\phi_j(x, z)$ for $j = 1, 2, 3, 4$ satisfies the governing partial differential equation given by

$$\left(\nabla_{xz}^2 - k_y^2 \right) \phi_j = 0 \tag{1}$$

where $\nabla_{xz}^2 = \left(\partial^2 / \partial x^2 + \partial^2 / \partial z^2 \right)$. The linearized free surface boundary condition is given by

$$\frac{\partial \phi_j}{\partial z} - K \phi_j = 0 \text{ on } z = 0, \text{ for } j = 1, 2, 3, 4, \tag{2}$$

where $K = \omega^2 / g$ and g is the acceleration due to gravity. Further, the rigid uniform bottom boundary condition is given by

$$\frac{\partial \phi_j}{\partial z} = 0 \text{ on } z = -h_i \tag{3}$$

where $i = 1$ for $j = 1$ and $i = 2$ for $j = 3, 4$. On the other hand, the bottom boundary condition for the undulated region 2 on $z = -h(x)$ is given by

$$\frac{\partial \phi_2}{\partial z} + \frac{dh}{dx} \frac{\partial \phi_2}{\partial x} = 0 \tag{4}$$

The horizontal velocity on the rigid wall vanishes, which is given as

$$\frac{\partial \phi_4}{\partial x} = 0 \text{ on } x = M_2 \tag{5}$$

where $M_2 = M_1 + D$ with $M_1 = L + L_1$. The flexible barrier is undertaken to be oscillating in the horizontal direction with a displacement of the form $\xi(y, z, t) = \text{Re} \left\{ \zeta(z) e^{-i(k_y y - \omega t)} \right\}$, where $\zeta(z)$ is the complex deflection amplitude of the flexible porous barrier. Thus, the boundary condition on the flexible porous barrier at $x = M_1$ is given by

$$\frac{\partial \phi_j}{\partial x} = ik_{10} G (\phi_3 - \phi_4) - i\omega \zeta, \text{ for } j = 3, 4, z \in H_b \tag{6}$$

where G is the complex porous-effect parameter as in Kaligatla et al. (2015). The equation of motion of the barrier acted upon by fluid pressure yields

$$EI \left(\frac{d^2}{dz^2} - k_y^2 \right)^2 \zeta + Q \left(\frac{d^2}{dz^2} - k_y^2 \right) \zeta - m_s \omega^2 \zeta = i\rho \omega (\phi_3 - \phi_4), \text{ } z \in H_b \tag{7}$$

Further, $EI = E d_s^3 / 12(1 - \nu^2)$ is the rigidity of the barrier, E is the Young modulus, d_s is the thickness of the barrier, ν is the Poisson ratio, Q is the uniform compressive force acting on the barrier, $m_s = \rho_s d_s$ is the uniform mass per unit length with ρ_s being the barrier density, and ρ is the density of water. The continuity of pressure and normal velocity along the gap is given by

$$\phi_3 = \phi_4, \quad \frac{\partial \phi_3}{\partial x} = \frac{\partial \phi_4}{\partial x}, \text{ on } x = M_1, \text{ } z \in H_g. \tag{8}$$

To keep the barrier in position and for the unique solution of the boundary value problem, four different types of edge conditions can be used, which are as follows:

- (i) Clamped-free: In this case, the barrier is assumed to be clamped at the upper end at $(M_1, 0)$ and free at the lower end at $(M_1, -a)$.
- (ii) Clamped-moored: In this case, the barrier is assumed to be clamped at the upper end at $(M_1, 0)$ and moored at the lower end at $(M_1, -a)$.
- (iii) Moored-free: In this case, the barrier is assumed to be moored at the upper end at $(M_1, 0)$ and free at the lower end at $(M_1, -a)$.
- (iv) Moored-moored: In this case, the barrier is assumed to be moored at the upper and lower ends at $(M_1, 0)$ and $(M_1, -a)$, respectively.
- (v) In the case of the clamped edge, barrier deflection and the slope of the barrier deflection will be vanished which are given as

$$\zeta(z) = 0, \zeta'(z) = 0 \text{ at } z = l_u, \tag{9}$$

while in the case of the moored edge, the bending moment will be vanished and the horizontal components of the

$$\left. \begin{aligned} \left(\frac{d^2}{dz^2} - \nu k_y^2\right)\zeta(z) &= 0 \\ \left[EI \left\{ \frac{d^2}{dz^2} - (2 - \nu)k_y^2 \right\} \frac{d}{dz} + Q \frac{d}{dz} \right] \zeta(z) &= 2K_m \sin^2(\sigma_m)\zeta(z) \end{aligned} \right\} \text{ at } z = l_u \tag{10}$$

where K_m is the mooring line stiffness and σ_m is the mooring line angle in the static position. It may be noted that for $\sigma_m = 0$, Eq. (10) will be the free edge condition at which the bending moment and shear force are zero. In Eqs. (9)–(10), l_u is 0, $-b$ as appropriate.

The far field boundary conditions are given by

$$\phi_1 = (I_0 e^{ip_{10}x} + R_0 e^{-ip_{10}x})f_{10}(k_{10}, z), \text{ as } x \rightarrow -\infty \tag{11}$$

where R_0 is the complex amplitude of the reflected wave and I_0 is the incident wave amplitude. Further, k_{10} is the real root of

dynamic mooring line tensions relate the restoring forces due to the axial load to the shearing forces, which are given as

the dispersion relation in region 1 with $p_{10} = \sqrt{k_{10}^2 - k_y^2}$ and $f_{10}(k_{10}, z)$ is the associated vertical eigenfunction.

3 Method of Solution

This section briefly describes the method of solution for the wave interaction with the surface-piercing flexible porous barrier in the presence of bottom undulation. Using the expansion formulae, the form of the spatial velocity potentials $\phi_j(x, z)$ for $j = 1, 2, 3, 4$ in each region is expressed as

$$\phi_j(x, z) = \begin{cases} I_0 e^{ip_{10}x} f_{10}(k_{10}, z) + \sum_{n=0}^{\infty} R_n e^{-ip_{1n}x} f_{1n}(k_{1n}, z), & x < 0, j = 1 \\ \sum_{n=0}^{\infty} \psi_n(x) W_n(h(x), z), & 0 < x < L, j = 2 \\ \sum_{n=0}^{\infty} (A_n e^{ip_{2n}x} + B_n e^{-ip_{2n}x}) f_{2n}(k_{2n}, z), & L < x < M_1, j = 3 \\ \sum_{n=0}^{\infty} T_n \cos p_{2n}(x - M_2) f_{2n}(k_{2n}, z), & M_1 < x < M_2, j = 4 \end{cases} \tag{12}$$

where $f_{in}(k_{in}, z)$ for $i = 1, 2$ and $n = 0, 1, 2, 3, \dots$ are the eigenfunctions and given as

$$f_{in}(k_{in}, z) = \frac{\cosh k_{in}(z + h_i)}{\cosh k_{in}h_i} \tag{13}$$

and $p_{in} = \sqrt{k_{in}^2 - k_y^2}$ with k_{10} and k_{20} are the positive real roots, k_{in} for $n = 1, 2, 3, \dots$ are the purely imaginary roots that satisfy the dispersion relation

$$\omega^2 = gk_{in} \tanh k_{in}h_i. \tag{14}$$

Further, in Eq. (12), $\psi_n(x)$ s are unknown functions and the eigenfunctions W_n are expressed as

$$W_n = \frac{\cosh \tilde{k}_{\sim n}(z + h)}{\cosh \tilde{k}_{\sim n}h} \tag{15}$$

where $\tilde{p}_n = \sqrt{\tilde{k}_n^2 - k_y^2}$. The wave number \tilde{k}_0 is a positive real root and $\tilde{k}_1, \tilde{k}_2, \tilde{k}_3, \dots$ are purely imaginary roots of the dispersion relation

$$\omega^2 = g\tilde{k}_{\sim n} \tanh \tilde{k}_{\sim n}h. \tag{16}$$

It may be mentioned that the roots $\tilde{k}_0, \tilde{k}_1, \tilde{k}_2, \tilde{k}_3, \dots$ are functions of the bottom profile $h(x)$ and the eigenfunctions W_n s which are borrowed from the flat bottom solution as in Porter and Staziker (1995). $R_n, A_n, B_n,$ and T_n are unknown constants to be determined. Hereafter, the infinite series associated with

the evanescent modes for the velocity potentials are truncated after N terms. Using the procedure of extended modified mild-slope equation (MMSE) as in Porter and Staziker (1995) to obtain $\psi_n(x)$ for the undulated region, it is derived that

$$\frac{d}{dx} \left(a_n \frac{d\psi_n}{dx} \right) + \sum_{m=0}^N \left[(b_{mn} - b_{nm}) \frac{dh}{dx} \frac{d\psi_m}{dx} + \left\{ b_{mn} \frac{d^2 h}{dx^2} + c_{mn} \left(\frac{dh}{dx} \right)^2 + d_{mn} - k_y^2 a_n \right\} \psi_m \right] = 0 \tag{17}$$

where

$$a_n(h) = \int_{-h}^0 W_n^2 dz, \quad b_{mn}(h) = \int_{-h}^0 W_n \frac{\partial W_m}{\partial h} dz, \\ c_{mn}(h) = \frac{db_{mn}}{dh} - \int_{-h}^0 \frac{\partial W_m}{\partial h} \frac{\partial W_n}{\partial h} dz, \quad d_{mn}(h) = \int_{-h}^0 W_n \frac{\partial^2 W_m}{\partial z^2} dz$$

for $n = 0, 1, 2, \dots, N$. Taking the velocity potential as in Eq. (12) and continuity of pressure across the interfaces $x = 0$ and $x = L$ yields

$$\left. \begin{aligned} \psi_0(x) &= I_0 e^{ip_{10}x} + R_0 e^{-ip_{10}x} \\ \psi_n(x) &= R_n e^{-ip_{1n}x} \end{aligned} \right\} \text{at } x = 0 \\ = 0 \text{ for } n = 1, 2, \dots, N \tag{18}$$

and

$$\psi_n(x) = A_n e^{ip_{2n}x} + B_n e^{-ip_{2n}x} \text{ at } x = L \text{ for } n = 0, 1, 2, \dots, N. \tag{19}$$

Using Eqs. (18) and (19) and the conservation of mass across the interface boundaries similar to Porter and Staziker (1995) at $x = 0$ and L brings out the jump conditions which are given by

$$\left. \begin{aligned} a_0 \frac{d\psi_0}{dx} + ip_{10} a_0 \psi_0 + h' \sum_{m=0}^N b_{m0} \psi_m - 2ip_{10} a_0 I_0 &= 0, \\ a_n \frac{d\psi_n}{dx} + ip_{1n} a_n \psi_n + h' \sum_{m=0}^N b_{mn} \psi_m &= 0, \end{aligned} \right\} \text{at } x = 0+, n = 1, 2, \dots, N \tag{20}$$

and

$$a_n \frac{d\psi_n}{dx} - ip_{2n} a_n \psi_n + h' \sum_{m=0}^N b_{mn} \psi_m - 2ia_n p_{2n} B_n e^{-ip_{2n}x} = 0 \text{ at } x = L-, n = 0, 1, 2, \dots, N. \tag{21}$$

Considering the velocity potentials ϕ_j for $j = 3, 4$ as in Eq. (12) and continuity of velocity conditions at $x = M_1$ as

in Eq. (8) along with the orthogonal characteristics of the eigenfunctions $f_{2n}(k_{2n}, z)$, the following is derived

$$A_n - B_n e^{-2ip_{2n}M_1} = -iT_n \sin p_{2n} D \text{ at } x = M_1, n = 0, 1, 2, \dots. \tag{22}$$

The plate deflection $\xi(z)$ is obtained by using Eq. (12) in Eq. (7),

$$\zeta(z) = \sum_{m=1}^4 C_m g_m(z) + \sum_{n=0}^{\infty} (e_n A_n + d_n T_n) f_{2n}(k_{2n}, z), \quad z \in H_b, \tag{23}$$

where $e_n = \beta_{1n} t_n$, $d_n = \beta_{2n} t_n$ with $\beta_{1n} = 2e^{-ip_{2n}M_1}$, $\beta_{2n} = i \sin p_{2n} D - \cos p_{2n} D$, $t_n = \frac{i\rho\omega}{EI p_{2n}^4 + Q p_{2n}^2 - m_s \omega^2}$, $g_1(z) = \frac{\cosh \tau_1 z}{\cosh \tau_1 h_2}$, $g_2(z) = \frac{\sinh \tau_2 z}{\sinh \tau_2 h_2}$, $g_3(z) = \frac{\sinh \tau_2 z}{\sinh \tau_2 h_2}$, and $g_4(z) = \frac{\sinh \tau_3 z}{\sinh \tau_3 h_2}$. Further, C_m (for $m = 1, 2, 3, 4$) are the unknowns and τ_n s are the roots of the characteristic equation $EI(\tau_n^2 - k_y^2)^2 + Q(\tau_n^2 - k_y^2) - m_s \omega^2 = 0$ with $\tau_n = i\tau_n$ for $n = 3, 4$. By making use of $\zeta(z)$ (from Eq. (23)) in Eq. (6), a series relation for the unknowns is derived as

$$\sum_{n=0}^{\infty} (H_n A_n + G_n T_n) f_{2n}(z) + i\omega \sum_{m=1}^4 C_m g_m(z) = 0, \text{ for } z \in H_b \tag{24}$$

where $H_n = i\omega e_n - ik_{10} G \beta_{1n}$ and $G_n = p_{2n} \sin p_{2n} D + i\omega e_n t_n - ik_{10} G t_n$. Moreover, using the continuity of the velocity potential as in Eq. (8) and the relations in Eq. (22), another series relation is obtained,

$$\sum_{n=0}^{\infty} (\beta_{1n} A_n + \beta_{2n} T_n) f_{2n}(z) = 0, \text{ for } z \in H_g. \tag{25}$$

The series relations in Eqs. (24) and (25) are satisfied in disjoint intervals and are referred to as dual series relations. These dual series relations are rewritten as

$$\mathcal{S}(z) = \sum_{n=0}^{\infty} \{ \mathcal{U}_n(z) + \mathcal{V}_n(z) T_n \} = 0, \quad -h_2 < z < 0 \tag{26}$$

where

$$\mathcal{U}_n(z) = \begin{cases} \beta_{1n} A_n f_{2n}(z), & \text{for } z \in H_g \\ H_n A_n f_{2n}(z) + \sum_{m=1}^4 C_m g_m(z), & \text{for } z \in H_b \end{cases} \\ \mathcal{V}_n(z) = \begin{cases} \beta_{2n} f_{2n}(z), & \text{for } z \in H_g, \\ G_n f_{2n}(z), & \text{for } z \in H_b, \end{cases}$$

and let $\mathcal{S}_N(z)$ be the N th partial sum of the series $\mathcal{S}(z)$. With help of the least squares approximation method, Eq. (26) can be written as

$$\int_{-h_2}^0 \mathcal{S}_M^*(z) \mathcal{S}_{T_n}(z) dz = 0, \quad \text{for } n = 0, 1, 2, 3, \dots, M \tag{27}$$

where $*$ denotes the complex conjugate and $\mathcal{S}_{T_n}(z)$ is the derivative of $\mathcal{S}_M(z)$ with respect to T_n . Thereafter, using Eq. (26) in Eq. (27), a system of linear equations is obtained as follows:

$$\sum_{m=0}^N T_m^* \mathcal{Y}_{mn} = \mathcal{J}_n, \quad \text{for } n = 0, 1, 2, \dots, M, \tag{28}$$

where

$$\begin{aligned} \mathcal{J}_n &= \int_{-h_2}^0 \mathcal{U}_n^*(z) \mathcal{U}_n(z) dz, \quad \mathcal{Y}_{mn} \\ &= \int_{-h_2}^0 \mathcal{V}_n^*(z) \mathcal{V}_n(z) dz, \quad \text{for } m, n \\ &= 0, 1, 2, \dots, M. \end{aligned} \tag{29}$$

Once and for all, Eq. (17) is solved using the fourth-order Runge-Kutta method to determine the unknown function ψ_n for specific bed profile $h(x)$. A system of $6N$ equations is derived from Eqs. (18)–(22) and (28) by using the computed values of ψ_n . Another four linear equations are obtained from the edge conditions as in Eqs. (9) and (10). The set of $6N + 4$ linear equations are then solved for the various physical quantities of interest.

4 Numerical Results and Discussion

In this section, we discuss results for a wide range of parameters, generated by a MATLAB code which has been

developed for investigating the effect of various wave and structural parameters on wave reflection, free surface elevations, and hydrodynamic forces on the barrier and rigid back wall. In the present study, time period $T = 8$ s, acceleration due to gravity $g = 9.81$ m/s², depth ratio $h_2/h_1 = 0.5$, $L/h_1 = 0.5$, $L_1/\lambda_1 = 0.5$, $D/\lambda_1 = 0.25$, $\lambda_1 = 2\pi/k_{10}$, $\gamma = EI/(\rho gh_2^4) = 0.01$, $\beta = Q/(\rho gh_2^2) = 0.1$, $\nu = m_s/(\rho h_2) = 0.1$, $\nu = 0.3$, $a/h_2 = 0.8$, $\sigma_m = 45^\circ$, $K_m = 10^3$ Nm⁻¹, and $\theta = 30^\circ$ are kept fixed unless it is mentioned otherwise. The reflection coefficient is defined by

$$K_r = \left| \frac{R_0}{I_0} \right| \tag{30}$$

The magnitude of the horizontal wave forces acting on the porous barrier K_f and on the rigid wall K_w is defined as

$$K_f = i\rho\omega \int_{-h_2}^0 \left\{ \phi_4(x, z) - \phi_3(x, z) \right\} \Big|_{x=M_1} dz, \tag{31}$$

$$K_w = i\rho\omega \int_{-h_2}^0 \phi_4(x, z) \Big|_{x=M_2} dz. \tag{32}$$

Further, the non-dimensional form of the horizontal wave forces on the barrier C_f and rigid wall C_w is derived using the formulae

$$C_f = \frac{|K_f|}{\rho gh_2^2} \quad \text{and} \quad C_w = \frac{|K_w|}{\rho gh_2^2}. \tag{33}$$

The undulated bed profile is considered using the bed function $h(x)$ as

$$\begin{aligned} h(x) &= h_1 - c \left\{ 1 - \alpha(1 - x/L)^2 + (\alpha - 1)(1 - x/L) \right\}, \quad 0 \\ &< x < L \end{aligned} \tag{34}$$

Fig. 2 Variation of K_r versus $k_{10}h_1$ for different values of **a** h_2/h_1 with $G = 1$ and **b** G with $h_2/h_1 = 0.5$. The other parameters are $\gamma = 5$, $\beta = 0$, $a/h_2 = 1$, $D/h_1 = 1$, $L/h_1 = 0.1$, and $\theta = 30^\circ$

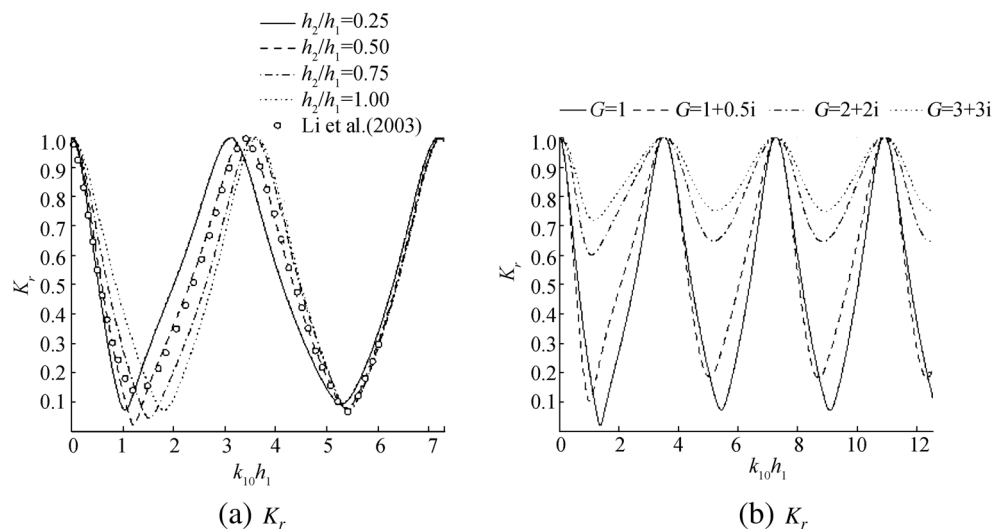
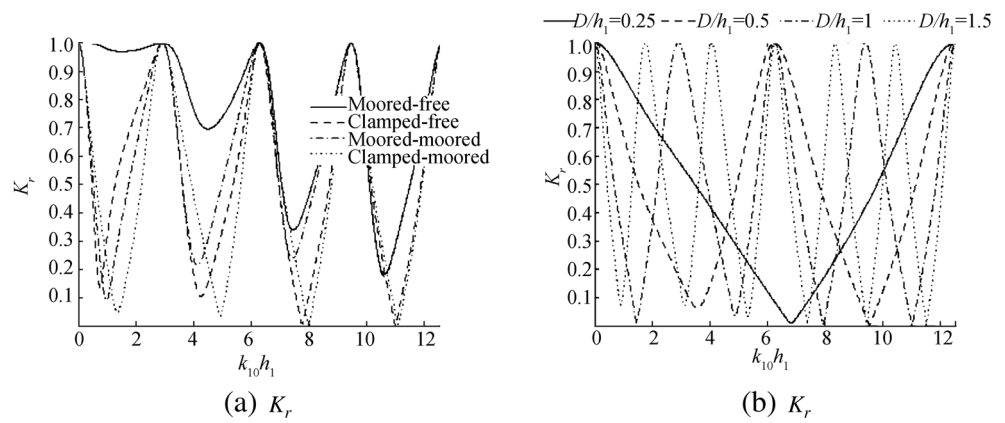


Fig. 3 Variation of K_r as a function of $k_{10}h_1$ for different **a** edge conditions with $D/h_1 = 1$ and **b** values of D/h_1 with the clamped-moored edge condition. For both panels, $\gamma = 0.01$, $h_2/h_1 = 0.5$, $\beta = 0$, $a/h_2 = 1$, $G = 1$, $L/h_1 = 0.1$, and $\theta = 0^\circ$



where $c = h_1 - h_2$. From the bed function $h(x)$ as in Eq. (34), various bed profiles can be obtained for different values of α such as the following: (i) $\alpha = 0$ refers to the sloping step-type bed, (ii) $\alpha > 1$ refers to the protrusion above the depth h_2 , (iii) for $-1 \leq \alpha < 0$ the bed is concave, and (iv) an increase in the depression of the bed profile will occur for $\alpha < -1$ (more details can be found in Behera et al. (2018)).

In Fig. 2a, b, the reflection coefficients K_r versus the non-dimensional wave number $k_{10}h_1$ are plotted for different values of depth ratio h_2/h_1 and porous-effect parameter G , respectively. In Fig. 2a, the results for $h_2/h_1 = 0.5$ and the larger rigidity of the fully extended barrier agrees well with the result of Li et al. (2003; Fig. 8) in the case of wave interaction with the porous barrier near a rigid wall in the presence of a vertical step. This figure shows that there is a right shift of full and minimum reflections with an increase in water depth for $k_{10}h_1 < 5.8$. However, for $k_{10}h_1 > 5.8$, there is a negligible effect of depth ratio h_2/h_1 in the wave reflection. From both figures, it is found that full reflection occurs periodically with an increase in $k_{10}h_1$. In the case of uniform water depth, full reflection occurs with a period 3.6, while in the presence of a step, the period decreases. With an increase in absolute value of the porous-effect parameter G , more wave energy passes through the porous barrier and is reflected by the rigid wall, and thus, the wave reflection increases with an increase in

absolute value of the porous-effect parameter as shown in Fig. 2b.

Reflection coefficients K_r against the dimensionless wave number $k_{10}h_1$ are plotted in Fig. 3a, b to check the effects of various edge conditions and the non-dimensional distance between the barrier and the rigid wall D/h_1 , respectively. Figure 3a depicts that the wave reflection is more in the case of the moored-free edge condition, whereas the wave reflection is less for the clamped-moored edge condition. This is due to the fact that in the case of the moored-free edge, more waves get transmitted through the barrier and then reflected by the rigid wall which results in more wave reflection as compared to the other edge conditions. However, the clamped-moored edge condition results in less flexibility at the edges of the barrier; thus, less waves get transmitted through the barrier and as a result, the wave reflection is less in this case. It may be noted that in other figures throughout the manuscript, the clamped-moored edge condition is used. Figure 3b shows that the number of full reflections increases due to the increase in distance between the barrier and rigid wall (D/h_1) with a period 0.25 of D/h_1 . It is also observed that for $D/h_1 \geq 0.5$ at $k_{10}h_1 = 6.2$, full reflection is obtained for each interval of $D/h_1 = 0.5$. Further, the wave reflection attains a minimum value between two consecutive wave numbers for which full reflection occurs.

Fig. 4 Variation of K_r with respect to D/λ_1 for different values of a/h_2 with $\beta = 0$, $G = 1$, $\theta = 30^\circ$, and $h_2/h_1 = 0.5$. **a** $\gamma = 5$ (rigid porous barrier). **b** $\gamma = 0.01$ (flexible porous barrier)

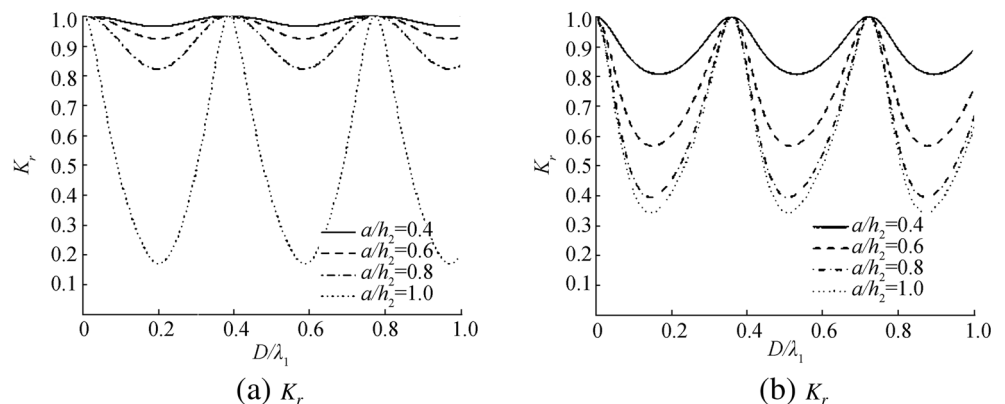
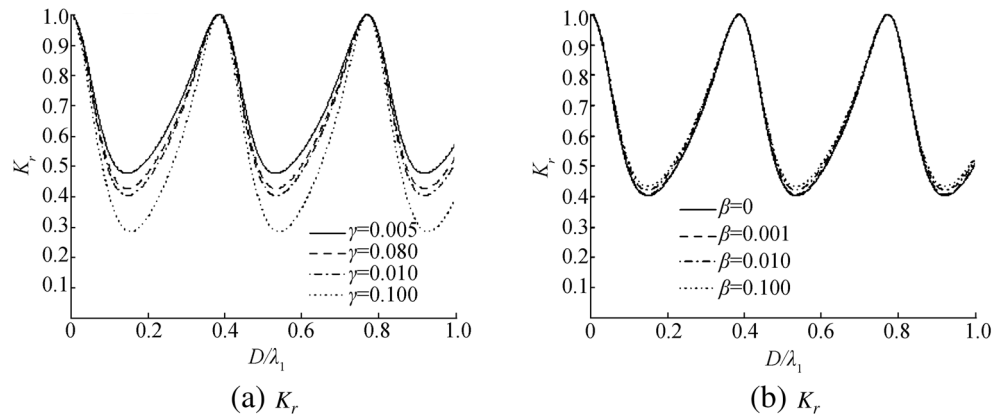


Fig. 5 Mutation of K_r as a function of D/λ_1 for **a** different γ with $\beta = 0$ and **b** different β with $\gamma = 0.01$, and in both, $h_2/h_1 = 0.5$, $a/h_2 = 0.8$, $G = 1$, and $\theta = 30^\circ$



The comparative study of the performance of (i) partial and fully extended and (ii) rigid and flexible porous barriers is presented in Fig. 4a, b. In Fig. 4a, the rigid porous barrier is considered, while the flexible porous barrier is considered in Fig. 4b with $\gamma = 0.01$. From both figures, it is seen that the reflection coefficient diminishes with an increase in the length of the barrier. This is due to the dissipation of more wave energy by the porous barrier as an increase in the length of the barrier. In the case of the rigid partial porous barrier (Fig. 4a), wave reflection is greater compared to the flexible partial porous barrier (Fig. 4b). However, in the case of the fully extended barrier ($a/h_2 = 1$), an opposite trend is observed. In literature, it is examined that in the case of a uniform bottom, full reflection is observed periodically when the distance between the porous barrier and the rigid wall becomes an integer multiple of half of the wavelength of the incident waves (see Yip et al. (2002) and Kaligatla et al. (2015)). However, from Fig. 4a, b, it is seen that in the presence of a step, full reflection can be found when the distance between the porous barrier and the rigid wall becomes an integer multiple of less than half of the wavelength of the incident waves. Moreover, it is observed that one minimum in the wave reflection occurs in between two consecutive maxima and it increases when the step height decreases.

The influences of non-dimensional flexural rigidity γ and compressive force β on the variation of reflection coefficients K_r are elaborated in Fig. 5a, b. It is observed that the reflection increases with increase of flexural rigidity as shown in Fig. 5a. Such a conclusion was also made earlier by Yip et al. (2002) and Kaligatla et al. (2015) in the case of wave trapping by flexible porous plates in a uniform water bottom. However, with an increase in compressive force β , the wave reflection increases.

Mooring angle ϑ and porous-effect parameter G are two monumental parameters. The dependence of the reflection coefficients K_r on ϑ and G (as a function of γ) is shown in Fig. 6a and b, respectively. From both figures, it is observed that the reflection coefficient decreases until it reaches a uniform pattern with an increase in the structural rigidity. Figure 6a shows that for less structural rigidity, wave reflection decreases with an increase of the mooring angle, while in the case of the highly flexible barrier, the mooring angle has a negligible effect on the wave reflection which may be due to the predominant role of higher modes of vibration of the highly flexible plate. On the other hand, with an increase in absolute value of the porous-effect parameter, the wave reflection increases as shown in Fig. 6b.

Fig. 6 Variation of K_r versus γ for different values of **a** σ_m with $G = 1$ and **b** G with $\sigma_m = 45^\circ$, when $h_2/h_1 = 0.5$, $a/h_2 = 0.8$, and $\theta = 30^\circ$

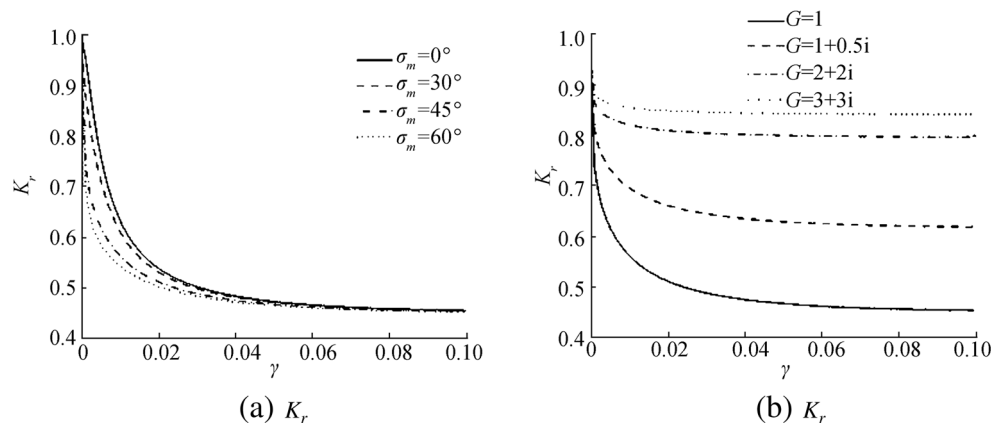
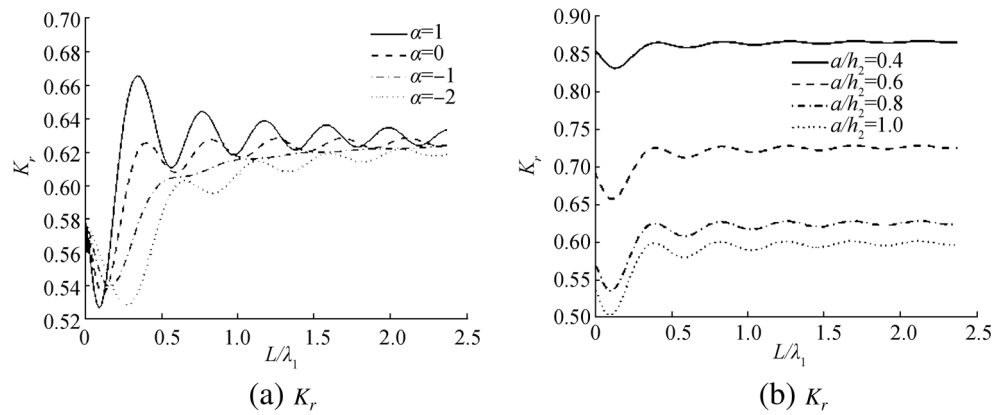


Fig. 7 Variation of K_r versus L/λ_1 for different values of **a** α with $a/h_2 = 0.8$ and **b** a/h_2 with $\alpha = 0$. The other parameters are $G = 1, \sigma_m = 45^\circ, h_2/h_1 = 0.5$, and $\theta = 30^\circ$



In Fig. 7a, b, the reflection coefficients K_r versus the non-dimensional slope length L/λ_1 are plotted for the different values' protrusion and depression parameter α of the bed function $h(x)$ and porous-effect parameter G , respectively. In the case of a larger sloping length, the water depth in all regions becomes the same; thus, with an increase in the sloping length, the oscillatory pattern of the wave reflection decreases as shown in both figures. Figure 7a depicts that wave reflection is greater in the case of protrusion in the step, while wave reflection is less for the step having depression. From Fig. 7b, it is manifested that the reflection coefficient decreases with an increase in length of the barrier which is because of the dissipation of more amount of wave energy by the porous barrier.

Figure 8 displays the parametric results in the $K_r - \theta$ plane system for two different values of water depth, $h_2/h_1 = 1$ (panel a) and $h_2/h_1 = 0.5$ (panel b). Figure 8a indicates that for $\theta = 0^\circ$, full reflection occurs periodically with the period $D/\lambda_1 = 0.5$ which follows the same as in Fig. 4a and is analogous to earlier results of Sahoo et al. (2000). However, full reflection does not occur at the same period in the presence of a step as shown in Fig. 8b. Moreover, in both cases, with an increase in D/λ_1 , the minimum of the wave reflection exponentially increases with respect to θ . It is also seen that the number of full reflections is less in the presence

of a step. Figure 8b shows that at $\theta = 72^\circ$, full reflection occurs at each interval $D/\lambda = 0.5$, and this angle is said to be a critical angle.

The changes of wave forces exerted on the barrier C_f and the rigid wall C_w versus the non-dimensional wave number k_{10} for several values of the porous-effect parameter G are plotted in Fig. 9a and b, respectively. In general, with an increase in G , more wave energy passes through the pores of the barrier; thus, the wave force decreases on the barrier and it increases on the rigid wall as the absolute value of the porous-effect parameter G increases. A comparison between Figs. 3b and 9a, b suggests the values of k_{10} for which full reflection occurs correspond to zero wave force on the barrier, and minimum reflection corresponds to maximum wave force on the rigid wall.

Panels a and b of Fig. 10 reveal the free surface elevations in open water (η_1/h_1) and confined (η_4/h_1) regions, respectively, for various values of the porous-effect parameter G . It is found that the amplitude of the free surface elevation in the confined region η_4/h_1 is less as compared to the open water region's free surface amplitude, which is due to the dissipation of wave energy by the porous structure. It is also seen that with an increase in the absolute value of the porous-effect parameter G , the amplitude of the free surface elevations decreases in both regions. In Fig. 10b, the deflection of the flexible barrier

Fig. 8 Change of K_r in terms of θ for different values of D/λ_1 in **a** $h_2/h_1 = 1$ and in **b** $h_2/h_1 = 0.5$ with $a/h_2 = 0.8, \alpha = 0, G = 1$, and $\sigma_m = 45^\circ$

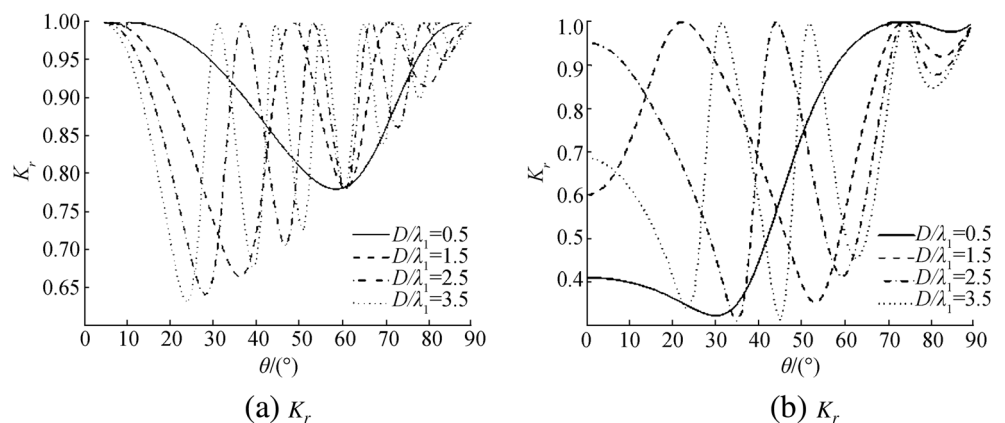
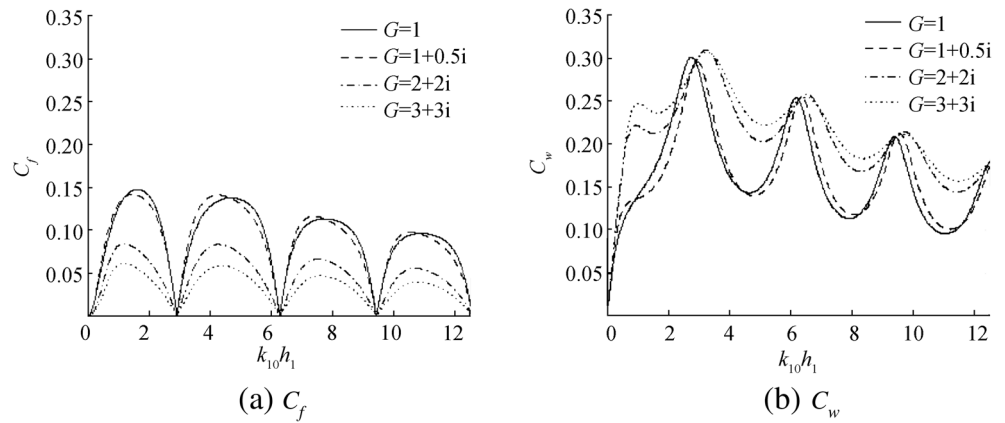


Fig. 9 Dependence of **a** C_f and **b** C_w on $k_{10}h_1$ for different values of G with $h_2/h_1 = 0.5$, $a/h_2 = 0.8$, $\alpha = 0$, $D/h_1 = 1$, $\theta = 30^\circ$, and $\sigma_m = 45^\circ$



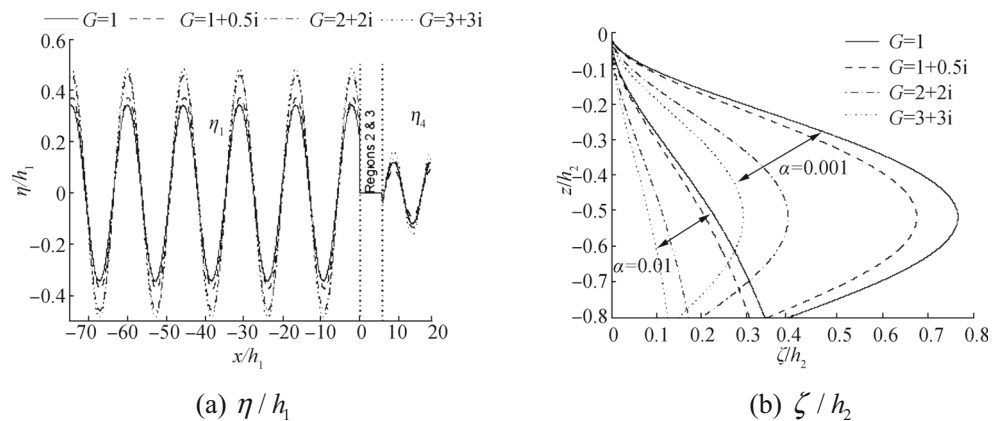
is plotted for various values of the porous-effect parameter G . It is observed that with an increase in the barrier rigidity γ , the barrier deflection decreases. Since the barrier is fixed near the free surface and moored near the submerged end, the deflection is zero at the upper end and non-zero at the other end. Moreover, the barrier deflection decreases with an increase in the absolute value of the porous-effect parameter.

5 Conclusion

The influence of a surface-piercing flexible porous barrier near a rigid wall in the presence of step-type bottoms is examined based on the linearized theory of water waves. The barrier is analyzed under (i) clamped-free, (ii) clamped-moored, (iii) moored-free, and (iv) moored-moored edge conditions to determine its preference as a breakwater in the lee side of the coastal region. The associated boundary value problem is solved by using the modified mild-slope approximation method along with the least squares approximation method. Numerical results are computed for reflection coefficients, free surface elevations, and wave forces on the barrier and the rigid wall. The computed results are validated with available results in the literature in the case of wave interaction with the flexible porous barrier near a rigid wall in uniform water

depth. The study reveals that the edge conditions play an important role not only for keeping the flexible barrier in position but also for the reduction of wave reflection. It is seen that the wave reflection is reduced for the clamped-moored barrier as compared to the barrier having the other edge conditions. Apart from uniform water depth, it is found that in the presence of a step, full reflection occurs periodically. However, the period for full reflection is less in the case of the step bottom as compared to the uniform bottom. It is observed that full reflection occurs in the period $D/h_1 = 0.25$ with an increase in the scaled wave number $k_{10}h_1$, and it is also seen that full reflection occurs in each interval at $k_{10}h_1 = 6.2$ for $D/h_1 \geq 0.5$. Further, at $k_{10}h_1 = 1.2$, nearly zero reflection occurs for certain values of wave and structural parameters, which is referred to as nearly full wave trapping in the confined zone. In the case of the uniform bottom, full reflection was obtained at $\theta = 0^\circ$ and $D/\lambda_1 = 0.5$, while it does not occur at $\theta = 0^\circ$ and $D/\lambda_1 = 0.5$ in the presence of a step. But full reflection was observed at each period of $D/\lambda_1 = 0.5$ when the angle $\theta = 72^\circ$. It is found that full reflection is associated with zero force on the barrier and maximum force on the rigid wall, and the maximum wave force on the barrier is associated with less force on the rigid wall. Further, in the confined region, the amplitude of the free surface elevation reduced significantly due to the dissipation of wave energy by

Fig. 10 Curves of **a** surface elevations η_j with $\gamma = 0.01$ and **b** barrier deflection ζ for different values of G with $h_2/h_1 = 0.5$, $a/h_2 = 0.8$, $\alpha = 0$, $\theta = 30^\circ$, and $\sigma_m = 45^\circ$



the porous barrier. Finally, the overall conclusion is that with a suitable combination of wave and structural parameters, the surface-piercing partial flexible porous barrier can be used as an effective breakwater, and the above important observations may help ocean engineers in the design of a perforated breakwater to create a calm region near sea walls, ports, and harbor walls.

References

- Behera H, Kaligatla R, Sahoo T (2015) Wave trapping by porous barrier in the presence of step-type bottom. *Wave Motion* 57:219–230. <https://doi.org/10.1016/j.wavemoti.2015.04.005>
- Behera H, Mandal S, Sahoo T (2013) Oblique wave trapping by porous and flexible structures in a two-layer fluid. *Phys Fluids* 25:112110. <https://doi.org/10.1063/1.4832375>
- Behera H, Ng CO (2018) Interaction between oblique waves and multiple bottom-standing flexible porous barriers near a rigid wall. *Meccanica* 53:871–885. <https://doi.org/10.1007/s11012-017-0789-8>
- Behera H, Sahoo T, Ng. CO (2016) Wave scattering by a partial flexible porous barrier in the presence of a step-type bottom topography. *Coast Eng J* 58:1650008. <https://doi.org/10.1142/S057856341650008X>
- Cho I, Kee S, Kim M (1998) Performance of dual flexible membrane wave barriers in oblique waves. *J Waterway Port Coastal Ocean Eng* 124:21–30. [https://doi.org/10.1061/\(ASCE\)0733-950X\(1998\)124:1\(21\)](https://doi.org/10.1061/(ASCE)0733-950X(1998)124:1(21))
- Chwang A, Dong Z, (1984) Wave-trapping due to a porous plate. In: *proc. 15th symposium on naval hydrodynamics*, pp: 407–417
- Huang Z, Li Y, Liu Y (2011) Hydraulic performance and wave loadings of perforated/slotted coastal structures: a review. *Ocean Eng* 38: 1031–1053. <https://doi.org/10.1016/j.oceaneng.2011.03.002>
- Jarlan G (1961) A perforated vertical wall breakwater. *Dock Harbour Authority* 41:394–398
- Kaligatla R, Koley S, Sahoo T (2015) Trapping of surface gravity waves by a vertical flexible porous plate near a wall. *Z Angew Math Phys*: 1–26. <https://doi.org/10.1007/s00033-015-0521-2>
- Karmakar D, Bhattacharjee J, Soares CG (2013) Scattering of gravity waves by multiple surface-piercing floating membrane. *Appl Ocean Res* 39:40–52. <https://doi.org/10.1016/j.apor.2012.10.001>
- Karmakar D, Soares CG (2014) Wave transformation due to multiple bottom-standing porous barriers. *Ocean Eng* 80:50–63. <https://doi.org/10.1016/j.oceaneng.2014.01.012>
- Koley S, Kaligatla R, Sahoo T (2015) Oblique wave scattering by a vertical flexible porous plate. *Stud Appl Math* 135:1–34. <https://doi.org/10.1111/sapm.12076>
- Koley S, Sahoo T (2017) Oblique wave trapping by vertical permeable membrane barriers located near a wall. *J Mar Sci Appl* 16:1–12. <https://doi.org/10.1007/s11804-017-1432-8>
- Liu Y, Li YC, Teng B, (2007a) The reflection of oblique waves by an infinite number of partially perforated caissons. *Ocean Eng* 34: 1965–1976. doi:<https://doi.org/10.1016/j.oceaneng.2007.03.004>
- Liu Y, Li Y, Teng B (2007b) Wave interaction with a new type perforated breakwater. *Acta Mechaica Sinica* 23:351–335. <https://doi.org/10.1007/s10409-007-0086-1>
- Li Y, Dong G, Liu H, Sun D (2003) The reflection of oblique incident waves by breakwaters with double-layered perforated wall. *Coast Eng* 50:47–60. <https://doi.org/10.1016/j.coastaleng.2003.08.001>
- Lo EY (1998) Flexible dual membrane wave barrier. *J Waterway Port Coastal Ocean Eng* 124:264–271. [https://doi.org/10.1061/\(ASCE\)0733-950X\(1998\)124:5\(264\)](https://doi.org/10.1061/(ASCE)0733-950X(1998)124:5(264))
- Lo EY (2000) Performance of a flexible membrane wave barrier of a finite vertical extent. *Coastal Eng J* 42:237–251. <https://doi.org/10.1142/S0578563400000110>
- Porter D, Staziker D (1995) Extensions of the mild-slope equation. *J Fluid Mech* 300:367–322. <https://doi.org/10.1017/S0022112095003727>
- Sahoo T, Lee M, Chwang A (2000) Trapping and generation of waves by vertical porous structures. *J Eng Mech* 126:1074–1082. [https://doi.org/10.1061/\(ASCE\)0733-9399\(2000\)126:10\(1074\)](https://doi.org/10.1061/(ASCE)0733-9399(2000)126:10(1074))
- Suh KD, Park WS (1995) Wave reflection from perforated-wall caisson breakwaters. *Coast Eng* 26:177–193. [https://doi.org/10.1016/0378-3839\(95\)00027-5](https://doi.org/10.1016/0378-3839(95)00027-5)
- Williams A (1996) Floating membrane breakwater. *J Offshore Mech* 118: 46–52 <https://offshoremechanics.asmedigitalcollection.asme.org/article.aspx?articleID=1453305>
- Yip TL, Sahoo T, Chwang AT (2002) Trapping of surface waves by porous and flexible structures. *Wave Motion* 35:41–54. [https://doi.org/10.1016/S0165-2125\(01\)00074-9](https://doi.org/10.1016/S0165-2125(01)00074-9)